Journal of Power Sources 266 (2014) 268–274

Contents lists available at ScienceDirect

Journal of Power Sources

journal homepage: www.elsevier.com/locate/jpowsour

Cathode supported tubular solid oxide fuel cells with nanostructured $La_{0.6}Sr_{0.4}Co_{0.2}Fe_{0.8}O_3$ electrocatalysts

Liuer Wu [a], Ling Zhao [a], Zhongliang Zhan [a, b], Changrong Xia [a, b, *]

[a] CAS Key Laboratory of Materials for Energy Conversion, Department of Materials Science and Engineering & Collaborative Innovation Center of Suzhou Nano Science and Technology, University of Science and Technology of China, Hefei, Anhui 230026, China
[b] Shanghai Institute of Ceramics, Chinese Academy of Sciences, Shanghai 200050, China

HIGHLIGHTS

- LSCF–YSZ cathode supported tubular SOFCs are successfully developed.
- The tubular cell has a low polarization resistance of 0.33 Ω cm^2 at 750 °C.
- The tubular cell has a peak power density of 0.55 W cm^{-2} at 750 °C.
- It is feasible to fabricate cathode supported SOFC with the impregnation method.

ARTICLE INFO

Article history:
Received 17 December 2013
Received in revised form
8 May 2014
Accepted 8 May 2014
Available online 20 May 2014

Keywords:
Solid oxide fuel cell
Tubular SOFC
Cathode substrate
Yttria stabilized zirconia
LSCF

ABSTRACT

Tubular solid oxide fuel cells (SOFCs) are developed with thick (~0.50 mm) $La_{0.6}Sr_{0.4}Co_{0.2}Fe_{0.8}O_3$ (LSCF) –$(Y_2O_3)_{0.08}(ZrO_2)_{0.92}$ (YSZ) cathode substrates and thin (6.9 μm) film YSZ electrolytes. LSCF is introduced to the thick porous YSZ substrate by impregnating technique, resulting in nanostructured LSCF particles, which are formed at 800 °C. The relatively low sintering temperature has effectively eliminated the possible solid–state reaction, which occurs between YSZ and LSCF above 900 °C. The nanostructured electrocatalyst promotes the electrochemical activity, resulting in total interfacial polarization resistance of 0.33 Ω cm^2 at 750 °C for the single cell. At the same temperature, the cell has achieved a peak power density of 0.55 W cm^{-2}, much higher than those reported for the cathode supported tubular SOFCs (about 0.2 W cm^{-2}). The improved performance demonstrates the feasibility of fabricating cathode supported tubular SOFCs with highly active catalysts such as LSCF, $Sm_{0.5}Sr_{0.5}CoO_3$, $Ba_{0.5}Sr_{0.5}Co_{0.8}Fe_{0.2}O_3$ and $PrBaCo_2O_5$.

1. Introduction

Tubular configuration has caused much attention as one of the solid oxide fuel cell (SOFC) designs, due to its particular advantages over the planar structure such as easier sealing and better thermal shock resistance [1,2]. The tubular SOFCs are mainly divided into four categories, which are supported on the anode, cathode and electrolyte in addition to porous metal substrates [3–7]. The cathode supported structures with thin anode layers have many advantages, especially when hydrocarbons are used as the fuels. In the thin-film anode, almost all the anode layer is electro-active, which is quite resistive to carbon deposition. In addition, the thin anode layer can reduce the volume contraction and expansion resulted from the accidental anode redox cycles. And also, the developed oxide anodes can be applied in the cathode supported configuration, replacing the Ni-based anodes, which undergo severe carbon deposition [8]. For a cathode supported SOFC operated with the methane fuel, redox-stable $La_{0.75}Sr_{0.25}Cr_{0.5}Mn_{0.5}O_3$ perovskite anode has been fabricated by slurry-printing and firing at only 950 °C to form a porous anode layer [9]. Therefore, the cathode supported tubular SOFCs are suitable for the new oxide anodes and potentially most reliable in the commercial application, which has been demonstrated by the outstanding reliability of Siemens' (formerly Westinghouse's) SOFC systems [10,11].

* Corresponding author. CAS Key Laboratory of Materials for Energy Conversion, Department of Materials Science and Engineering & Collaborative Innovation Center of Suzhou Nano Science and Technology, University of Science and Technology of China, Hefei, Anhui 230026, China. Tel.: +86 551 63607475; fax: +86 551 63601696.
E-mail address: xiacr@ustc.edu.cn (C. Xia).

http://dx.doi.org/10.1016/j.jpowsour.2014.05.055
0378-7753/

The cathode supported tubular SOFCs have been reported mainly using $LaMnO_3$-based cathodes and zirconia-based electrolytes [12,13]. Although the cell configuration seems attractive, the performance is relatively low. This can be ascribed to the following three reasons. Firstly, (La, Sr)MnO_3 (LSM)-based materials are electronic conductors with negligible ionic conductivity and poor electrochemical activity to oxygen reduction [14]. Secondly, the cathode substrate and the electrolyte have to be co-sintered at high temperatures (above 1200 °C) to densify the electrolyte and achieve the mechanical strength during the fabrication routes. Such high temperature may induce the chemical reactions or element diffusion, resulting in electric degradation at the cathode/electrolyte interfaces. Thirdly, the high temperature co-sintering process can promote the adverse coarsening of the cathode particles, resulting in the loss of triple phase boundaries (TPBs) for oxygen reduction. Hence, to achieve high performance, cathode material with high catalytic activity should be used to replace the LSM-based materials. In addition, particle coarsening should be avoided in the fabrication process. Comparing with LSM, cobaltite based oxides such as $La_{0.6}Sr_{0.4}Co_{0.2}Fe_{0.8}O_3$ (LSCF), $Sm_{0.5}Sr_{0.5}CoO_3$ (SSC), $Ba_{0.5}Sr_{0.5}Co_{0.8}Fe_{0.2}O_3$ (BSCF) and $PrBaCo_2O_5$ (PBC) are much superior cathode materials due to their higher oxygen ionic conductivity and electro-catalytic activity [15–18]. However, the application is limited by the poor chemical compatibility with zirconia-based materials. For example, LSCF reacts with yttria stabilized zirconia (YSZ) at 900 °C, much lower than the desired sintering temperature (~1400 °C) to densify YSZ electrolytes [19]. Therefore, a practical fabrication method should be proposed to prepare catalytically active cathode supporters and meanwhile to avoid the possible solid-state reaction induced by high temperature sintering in the fabrication process.

In this work, a fabrication method is demonstrated to prepare the cathode supported tubular SOFCs with YSZ electrolytes and LSCF-based cathodes. The LSCF particles are introduced to the cathode supporters using the well-developed impregnation/infiltration technique, which is a low-temperature preparation method to prepare nanostructured electrodes [20]. The impregnation method is used to introduce LSCF particles into porous YSZ tubular substrate to prepare the cathode, which is about 0.5 mm thick. The tubular substrate contains a highly porous thick YSZ layer and a dense thin YSZ layer, which is derived from a NiO–YSZ/YSZ bi-layer structure. Preparation of the NiO–YSZ/YSZ tubes is relatively facile since NiO is chemically compatible with YSZ [21] and the relevant techniques such as extrusion and dip-coating are much mature [22,23]. LSM based cathodes are also prepared using the same procedure for comparison.

2. Experimental

2.1. Preparation of cathode supported tubular cell

Fig. 1 schematically represents the route to fabricate the cathode supported tubular SOFC. The route generally consists of three parts. Firstly, a thin dense YSZ electrolyte is fabricated on a porous YSZ substrate, which is derived from NiO–YSZ, where NiO is used as the pore former. The tubular NiO–YSZ/YSZ structure was formed by a simple dip-coating and co-sintering method, which is well developed and often applied in fabricating anode supported tubular SOFCs [23,24]. Details of the method are reported by Liu et al. [23]. Unless otherwise specified, all the starting chemicals were from Sinopharm Chemical Reagent Co. Ltd. The NiO–YSZ substrate consisted of 50 wt.% NiO (Lanzhou Jinchuan Metal Material Technology Co., China) and 50 wt.% YSZ (Farmeiya Advanced Materials Co., China). Fine YSZ (TOSOH Co.) powder was used to fabricate the thin electrolyte layer. The resulted tube is approx. 2.5 cm long, 1.0 cm in outside diameter, and 0.50 mm thick.

NiO was removed by a chemical method. The NiO–YSZ tube with dense YSZ electrolyte was reduced to Ni–YSZ at 750 °C for 5 h in H_2–H_2O (3% H_2O) stream. Ni was then completely removed by soaking the Ni–YSZ/YSZ tube in a 4 mol L^{-1} nitric acid solution at 70 °C for 10 h. After washing with distilled water and drying, a white tube was obtained with a thick (~0.50 mm) porous YSZ layer and a thin (~7 μm) dense YSZ layer, i.e. porous-YSZ/dense-YSZ bilayer, Fig. 1.

Secondly, NiO–YSZ (TOSOH Co.) anode was applied on to the YSZ electrolyte by brush-painting. NiO powder was synthesized via a glycine nitrate method [25]. NiO–YSZ slurry was prepared by mechanically mixing the NiO and YSZ powders (at a weight ratio of 3:2) with organic additives such as terpilenol and ground with agate mortar. The NiO–YSZ slurry was then painted on to the YSZ electrolyte and heated at 1200 °C for 2 h in air, resulting in a porous-YSZ/dense-YSZ/NiO–YSZ tri-layer structure, Fig. 1. The anode active area was about 0.6 cm^2.

Finally, LSCF was impregnated to the porous YSZ layer to form LSCF–YSZ cathode. The impregnation cycle was conducted by pouring into the tube with 0.5 mol L^{-1} $La_{0.6}Sr_{0.4}Co_{0.2}Fe_{0.8}O_3$ solution, vacuum-pumping, pouring out, drying, and firing at 800 °C for 2 h in air. The LSCF solution was prepared by dissolving stoichiometric amounts of $La(NO_3)_3$, $Sr(NO_3)_2$, $Co(NO_3)_2$, and $Fe(NO_3)_3$ in distilled water, to which citric acid and EDTA were added with a citric acid, EDTA to nitrate molar ratio of 1:1:1. The LSCF loading was determined using electronic balance (AB135-S, Mettler Toledo). The loading for each impregnation cycle is about 13 mg LSCF per gram YSZ. $(La_{0.85}Sr_{0.15})_{0.95}MnO_3$ (LSM) was also impregnated to the porous YSZ substrate via the same processes as the LSCF impregnation. The LSM solution was 0.5 mol L^{-1} and consisted of $La(NO_3)_3$, $Sr(NO_3)_2$, $Mn(NO_3)_2$ and glycine with a glycine to nitrate molar ratio of 0.5. For each impregnation cycle, LSM was fired at 800 °C for 2 h, and the loading was about 16 mg per gram YSZ.

2.2. Characterization

Single phase LSCF powder was prepared for structure analysis by heating the LSCF solution on a hot plate till self-ignition, producing a highly porous black metal-oxide ash, which was collected and heated at 800 °C for 2 h. The LSCF powder was then mixed with YSZ powder at a mass ratio of 1:1, and heated at 800 °C for 2 h. The mixture was named as mixed LSCF–YSZ powder. Impregnated LSCF–YSZ powder was also prepared by crushing and milling the LSCF impregnated YSZ tube. The powders were analyzed using X-ray diffraction (XRD, D/Maxra) equipped with Cu Kα radiation. The pore size distributions of anode supporters were measured with mercury porosimetry (Model PM60GT-17, Quantachrome Instrument). The microstructure was characterized by scanning electron microscopy (SEM, JSM-6700F).

For fuel cell tests, the tubular cell was sealed to quartz tube with electric conductive adhesive (DAD-87, Shanghai Synthetic Resin Institute), Fig. 2. Ag paste (Sino-platinum Metals Co., Ltd) was painted on both the anode and cathode surface as the current collector. A four-probe setup was used to eliminate the resistive losses in the Ag current-collecting wires. The single cell was tested in a tube furnace at temperatures from 600 to 750 °C, using humidified hydrogen (70 ml min^{-1}) as the fuel and flowing air (100 ml min^{-1}) as the oxidant. The voltage–current curves were measured using a Zahner Zennium electrochemical station, as well as the impedance spectra under open circuit conditions with amplitude of 10 mV over the frequency range from 1 MHz to 0.1 Hz. The cell stability was recorded using a potentiostat (CHI 1100A, Chenhua, Shanghai).

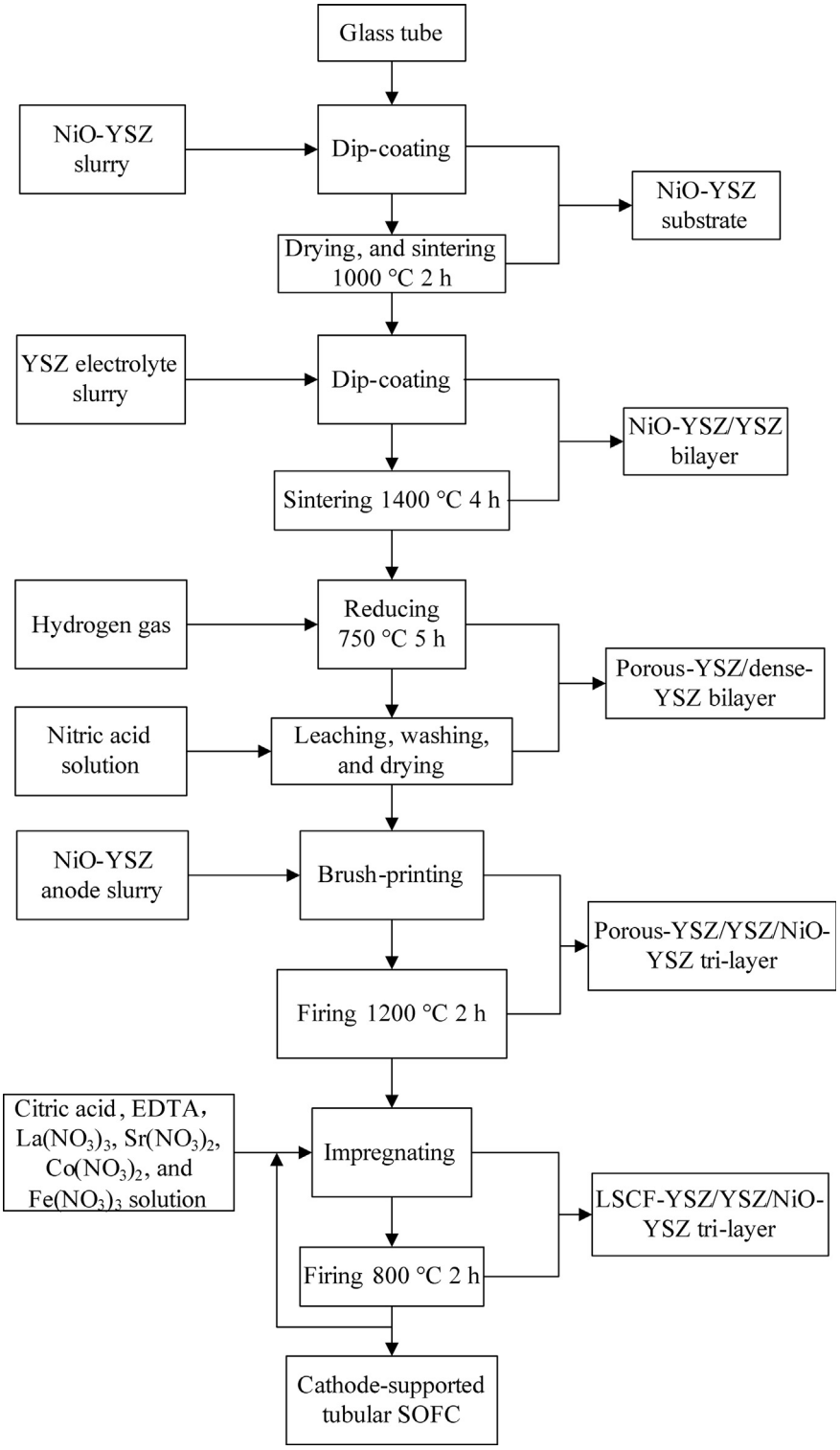

Fig. 1. Fabrication route for the LSCF–YSZ supported tubular SOFC where nanostructured LSCF is prepared by an impregnation method.

3. Results and discussion

The tubular porous-YSZ/dense-YSZ bilayer substrate possesses a fine fluorite structure and no other phase can be found within the sensitivity of XRD, Fig. 3a. This implies the excellent chemical compatibility between NiO and YSZ when they are co-sintered at 1400 °C. No residual nickel is observed after the chemical treatment, demonstrating NiO is a favorite pore generator [26] for preparing porous YSZ especially considering the mature technique of fabricating NiO–YSZ/YSZ bi-layers. Fig. 3b is the diffraction pattern for the LSCF powder, which is prepared by heating the LSCF solution and firing at 800 °C. The pattern presents the perovskite structure. The XRD pattern for the LSCF infiltrated YSZ supporter can be ascribed to either LSCF or YSZ without any other unexpected

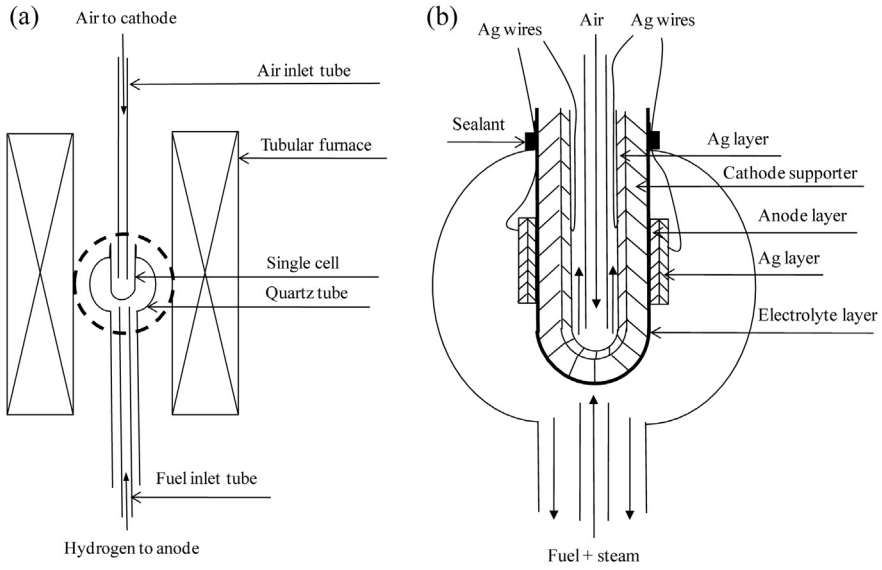

Fig. 2. Experimental setup: (a) schematic arrangement for testing the cathode supported single cell and details in the dashed circle are shown in (b).

phase, Fig. 3c. This shows that the perovskite phase is also formed when the impregnated LSCF is heated at 800 °C for 2 h. In addition, no obvious impurity phase is observed when LSCF is formed on the YSZ skeleton under the experimental conditions. However, the peak intensity for LSCF is much smaller than YSZ since the LSCF content is about 15 wt.% in the impregnated LSCF–YSZ powder. Fig. 3d shows the XRD pattern for the mixed LSCF–YSZ powder with 50 wt.% LSCF. All the peaks could be attributed to either LSCF or YSZ, demonstrating no obvious solid state reaction between LSCF and YSZ at the temperature for LSCF cathode fabricating, consistent with the results reported by Chen et al. [27].

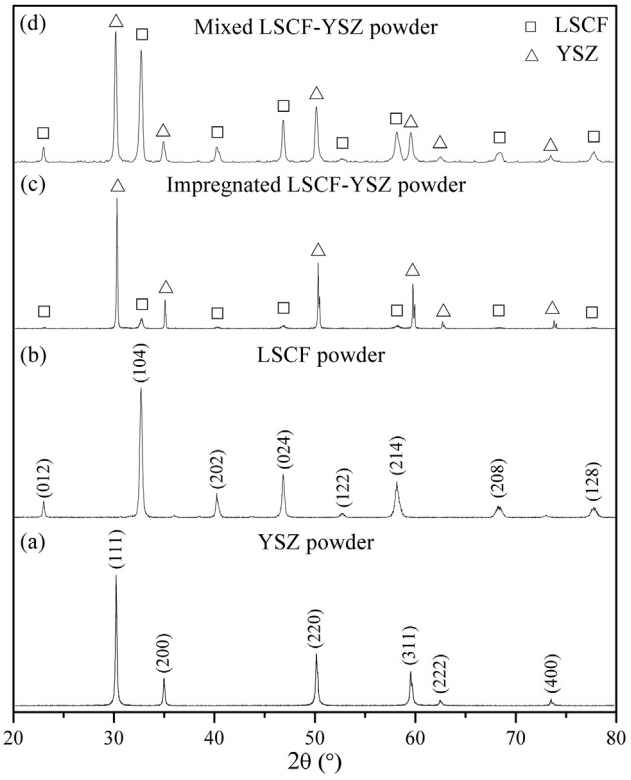

Fig. 3. Room temperature XRD patterns for (a) YSZ powder derived from porous-YSZ/dense-YSZ bilayer, (b) LSCF powder from LSCF solution, (c) impregnated LSCF–YSZ powder, and (d) mixed LSCF–YSZ powder heated at 800 °C.

Fig. 4a shows the microstructure of the porous YSZ substrate. Homogeneous pore distribution presents when NiO is removed. The porosity is about 50%. The mean pore diameter is 0.41 μm, Fig. 5. After impregnation with LSCF, the porosity decreases, Fig. 4b. It is to about 35%. The mean pore diameter decreases to 0.36 μm. And the pore distribution becomes broader, Fig. 5. Fig. 4c displays a typical cross-sectional SEM image of a single cell consisting of the LSCF infiltrated YSZ cathode, YSZ electrolyte and Ni–YSZ anode. The thicknesses of the YSZ electrolyte and the Ni–YSZ anode are about 6.9 μm and 14.2 μm, respectively. The electrolyte layer appears fully dense with only a few isolated pores. The Ni–YSZ anode is porous and contacts well with YSZ electrolyte, Fig. 4d. The good contact could facilitate the oxygen ionic transport across the anode/electrolyte interface. Fig. 4e and f present the microstructures of the LSCF infiltrated YSZ after long time test. On the YSZ surface, a close coating layer presents with well interconnected LSCF particles, which could promote the electric conduction and hence decrease the cathode ohmic resistance. The average size of the LSCF particle is about 170 nm, Fig. 4f. The small particle size is favorable to the catalytic activity since small size means rich TPB sites where oxygen reduction reaction occurs [28].

Fig. 6a presents the current–voltage (I–V) and current–power density (I–P) curves at 750 °C. The open circuit voltage (OCV) values are close to 1.1 V, indicating that the YSZ electrolyte layer is dense enough to prevent the cross-over of the fuel and air. When stationary air is used as the oxidant, the cell exhibits a limited performance with a peak power density of 0.44 W cm^{-2} since severe concentration polarization is observed when the current density exceeds 0.85 A cm^{-2}. This seems to be due to the thick cathode with impregnated structure. In the previous report, most of the impregnation effort is devoted to prepare thin-layer cathodes for the planar SOFCs, where the cathode is about 20–60 μm thick. When ambient air is used, no obvious concentration polarization has been observed for the planar single cells with 60-μm-thick LSM impregnated cathode [29] and 50-μm-thick LSCF impregnated cathode [30] at a current density up to 1 A cm^{-2}. The peak power density increases to 0.55 W cm^{-2} when 100 ml min^{-1} air is used. And no concentration polarization is observed even when the

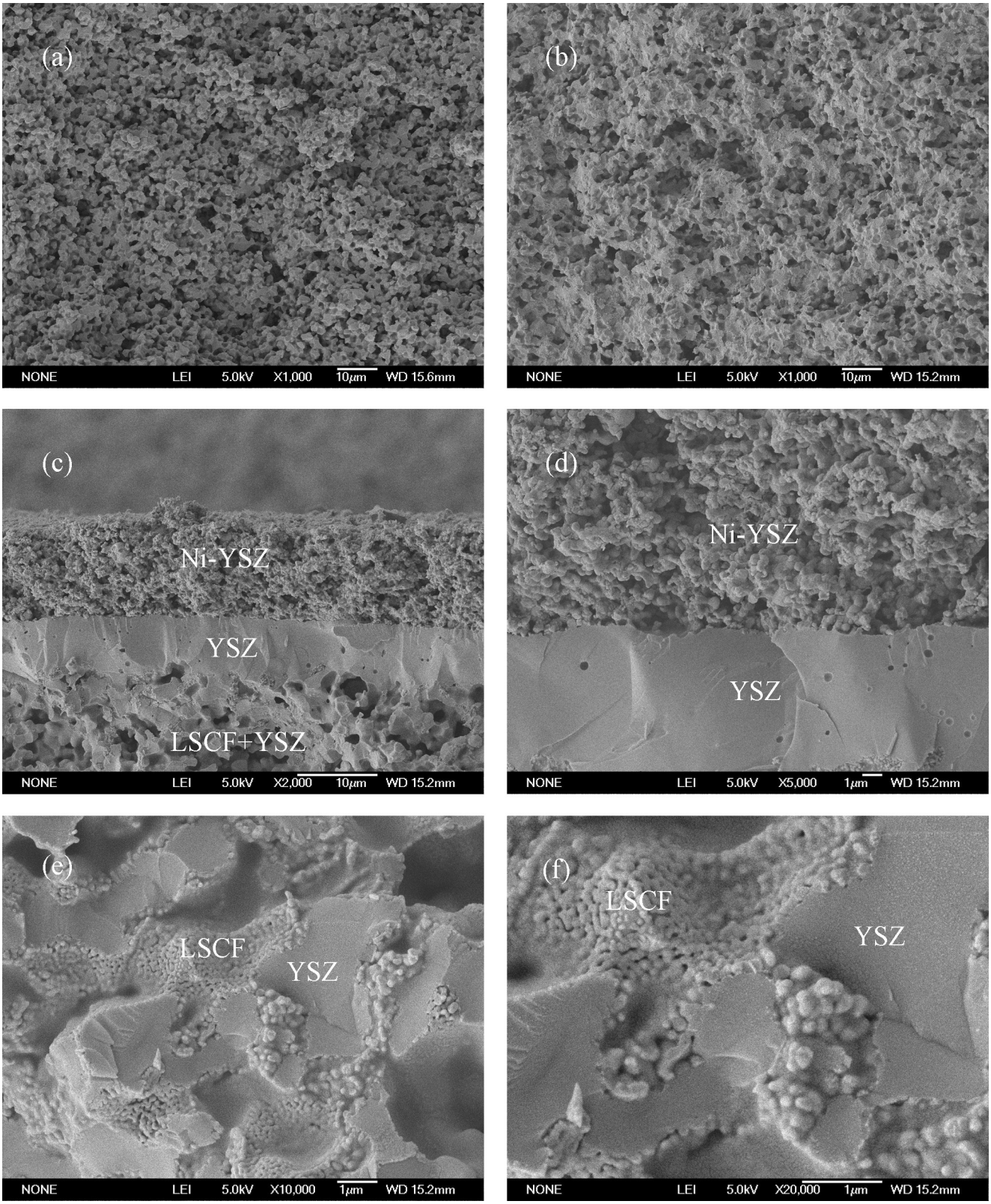

Fig. 4. Cross-sectional images for (a) a blank porous YSZ; (b) a porous YSZ infiltrated with LSCF; (c) a three-layer single cell; (d) the anode/electrolyte interface; (e) LSCF particles coated on the inner surface of porous YSZ, and (f) viewed at a higher magnitude.

current density reaches 1.6 A cm^{-2}. Fig. 6b shows the impedance spectra under open-circuit conditions using stationary air and flowing air. The total polarization resistance remains unchanged, 0.33 Ω cm^2 at 750 °C, suggesting the concentration polarization cannot be clearly distinguished under the open-circuit conditions.

Fig. 7 shows the cell performance at different temperatures using flowing air as the oxidant. The terminal voltage exhibits a

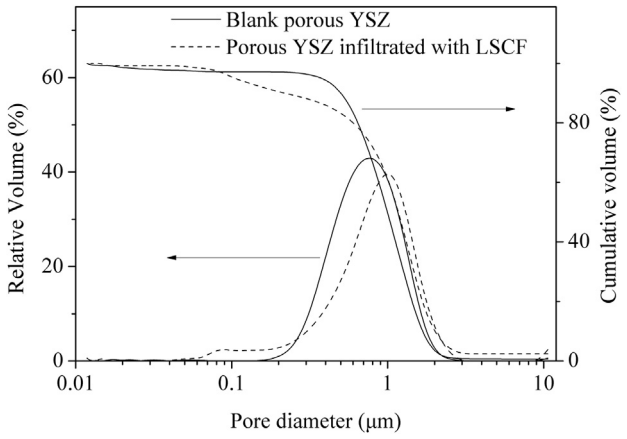

Fig. 5. Pore size distributions for a blank porous YSZ supporter as shown in Fig. 4a and a LSCF infiltrated supporter as shown in Fig. 4b.

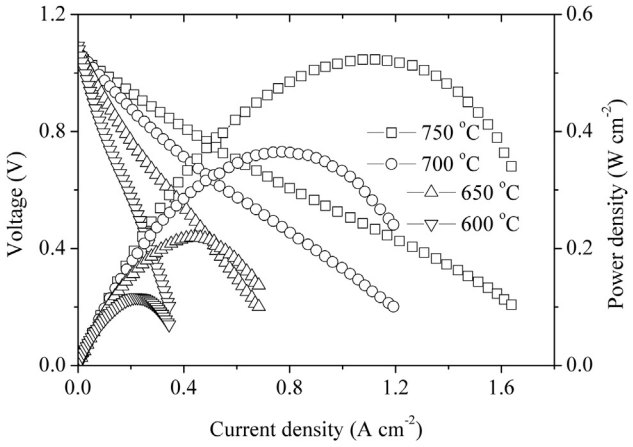

Fig. 7. *P–V–I* curves measured at different temperatures.

linear decrease with the increasing current density. The area specific resistance (ASR) for the single cell is calculated to be 0.54 Ω cm^2 at 750 °C and 2.59 Ω cm^2 at 600 °C from the slope of the voltage–current curves. The peak power densities are 0.55, 0.37, 0.22, 0.12 W cm^{-2} at 750, 700, 650, and 600 °C, respectively. The performance is higher than those reported for cathode supported tubular SOFCs using humidified H_2 as the fuel [31–34]. Zhao et al. have reported a peak power density of 0.15 W cm^{-2} at 750 °C for the cathode supported tubular cell with LSM/LSM–$Zr_{0.89}Sc_{0.1}Ce_{0.01}O_2$ (SSZ)/SSZ/Ni–SSZ structure [31]. For a $La_{0.6}Ca_{0.3}Ce_{0.1}Mn_{0.99}(Ni,Cr)_{0.01}O_3$/SSZ/Ni–SSZ based commercial cathode supported tubular SOFC, the maximum performance reaches about 0.18 W cm^{-2} at 700 °C when Sm-doped CeO_2 electrocatalysts are infiltrated to both the cathode and anode [32].

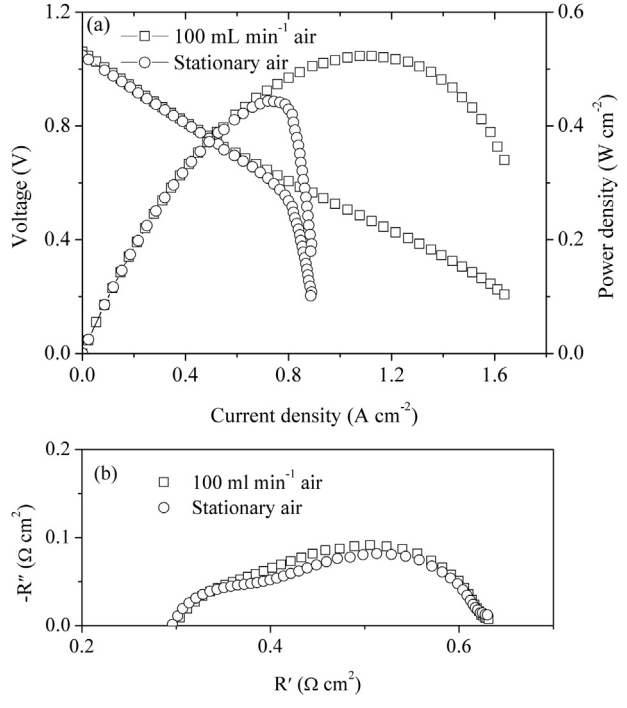

Fig. 6. (a) *P–V–I* curves and (b) impedance spectrum under open-circuit conditions measured at 750 °C for the single cell using stationary and flowing air as the oxidant.

Fig. 8a and b shows the electrochemical impedance spectra for the single cell measured under open circuit conditions from 750 to 600 °C. Flowing air is used as oxidant. Ohmic resistance (R_o) is 0.31 Ω cm^2 at 750 °C, and increases to 0.62 Ω cm^2 at 600 °C. R_o values are much higher than the estimated ohmic resistance (0.04 Ω cm^2 at 750 °C) for the 6.9 μm thick YSZ layer using the conductivity reported by Ciacchi et al. [35]. The ohmic resistance is contributed by not only the electrolyte, but also the electrodes and the electrolyte/electrode interfaces. In this cathode supported configuration, R_o may be related to the cathode supporter in addition to the electrolyte. The electrode polarization resistance (R_p), including both the anode and the cathode contribution, is 0.33 and 2.91 Ω cm^2, respectively, at 750 and 600 °C. In the previous report, a LSM/LSM-SSZ cathode supported tubular cell consisted of 10-μm-thick SSZ electrolyte and Ni-SSZ anode exhibits R_o of 0.91 Ω cm^2, R_p of 1.84 Ω cm^2 [31]. In comparison, R_o and R_p of our configuration are much lower, leading to the high power density. The total resistance (R_t) is the sum of R_o and R_p, 0.64 and 3.53 Ω cm^2 at 750 and 600 °C, respectively. At the same temperature, R_t is higher than the resistance estimated from the *V–I* curve. The difference is usually caused by the activation polarization [36]. The contribution of R_p to R_t is 51% at 750 °C, increases to 82% at 600 °C.

Fig. 9 shows the performance of a LSM (15 wt.%) infiltrated YSZ cathode supported tubular cell. At 750 °C, the peak power density is about 0.17 W cm^{-2} (Fig. 9a), higher than that reported for an LSM-based cathode supported tubular cell, 0.15 W cm^{-2} [31], but much lower than that of the LSCF-based cell, 0.55 W cm^{-2}. From the

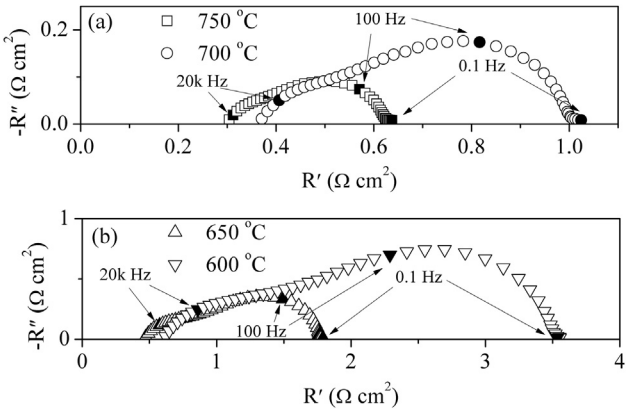

Fig. 8. Impedance spectra measured under open circuit conditions.

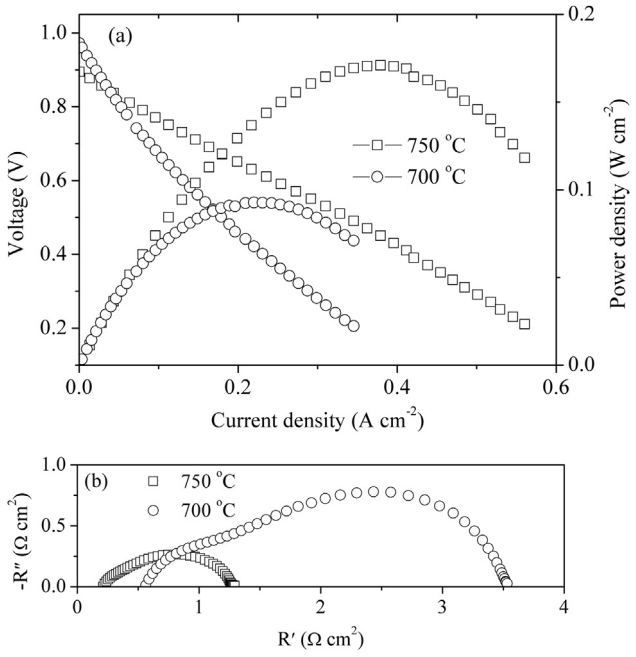

Fig. 9. The performance for a LSM-infiltrated cathode-supported tubular cell: (a) *P–V–I* curves and (b) impedance spectrum under the open-circuit conditions.

impedance spectrum (Fig. 9b), the ohmic resistance is close to that of the LSCF cell. However, the polarization resistance is much higher. At 700 °C, R_p is about 3 Ω cm^2, five times higher than that of the LSCF-based cell.

Fig. 10 shows the current density versus the testing time when the cell is operated with a constant voltage load (0.7 V) at 600 °C. Within the tested 220 h, a relatively flat performance is observed, with a decline of about 3%.

4. Conclusions

LSCF–YSZ cathode supported tubular solid oxide fuel cells are successfully fabricated by impregnating LSCF solution into porous YSZ supported tube. No obvious solid state reaction is observed between LSCF and YSZ due to the relatively low processing temperature. Well connected LSCF particles of nano-scale are formed on the inner surface of the porous YSZ. The cell has possessed low ohmic and polarization resistance, 0.31 Ω cm^2 and 0.33 Ω cm^2 at 750 °C, respectively. The peak power densities are 0.55, 0.37, 0.22, 0.12 W cm^{-2} at 750, 700, 650, and 600 °C, respectively. The power density is about three times higher than that of the LSM-infiltrated cathode-supported tubular cell. While extensive concern is now focused on the co-sintering process of the cathode supporter and the electrolyte, our results demonstrate a feasible approach for fabricating cathode supported tubular cell with high catalytic materials such as LSCF, SSC, BSCF and PBC.

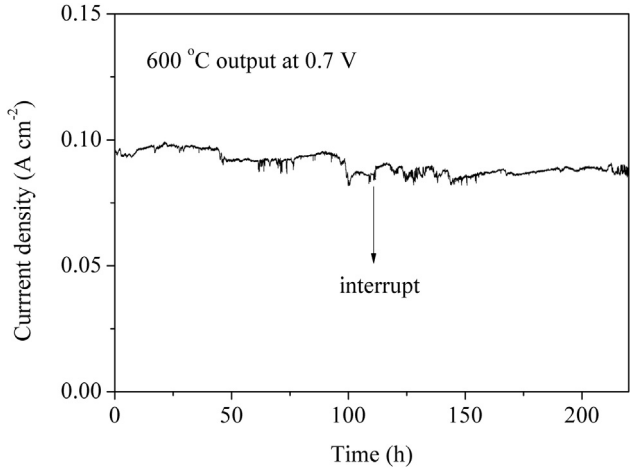

Fig. 10. Stability test of the single cell at 600 °C and 0.7 V.

Acknowledgments

We thank gratefully the financial support of the Ministry of Science and Technology of China (2012CB215403) and the National Natural Science Foundation of China (51372239).

References

[1] K. Kendall, M. Palin, J. Power Sources 71 (1998) 268–270.
[2] N.M. Sammes, Y. Du, R. Bove, J. Power Sources 145 (2005) 428–434.
[3] Y. Du, N.M. Sammes, J. Power Sources 136 (2004) 66–71.
[4] T. Yamaguchi, S. Shimizu, T. Suzuki, Y. Fujishiro, M. Awano, Mater. Lett. 62 (2008) 1518–1520.
[5] H. Kim, A. Parfitt, S.T. Park, Y.S. Chung, J.S. Chung, N.M. Sammes, ECS Trans. 57 (2013) 683–689.
[6] W.S. Hsieh, P. Lin, S.F. Wang, Int. J. Hydrogen Energy 38 (2013) 2859–2867.
[7] M.C. Tucker, G.Y. Lau, C.P. Jacobson, L.C. DeJonghe, S.J. Visco, J. Power Sources 175 (2008) 447–451.
[8] T. Takeguchi, Y. Kani, T. Yano, R. Kikuchi, K. Eguchi, K. Tsujimoto, Y. Uchida, A. Ueno, K. Omoshiki, M. Aizawa, J. Power Sources 112 (2002) 588–595.
[9] X.J. Chen, Q.L. Liu, S.H. Chan, N.P. Brandon, K.A. Khor, Electrochem. Commun. 9 (2007) 767–772.
[10] R.A. George, J. Power Sources 86 (2000) 134–139.
[11] K. Huang, S.C. Singhal, J. Power Sources 237 (2013) 84–97.
[12] H. Orui, K. Watanabe, M. Arakawa, J. Power Sources 112 (2002) 90–97.
[13] T. Matsui, J.Y. Kim, H. Muroyama, M. Shimazu, T. Abe, M. Miyao, K. Eguchi, Solid State Ionics 225 (2012) 50–54.
[14] Y. Wang, L. Zhang, C.R. Xia, Int. J. Hydrogen Energy 37 (2012) 2182–2186.
[15] J.A. Lane, S.J. Benson, D. Waller, J.A. Kilner, Solid State Ionics 121 (1999) 201–208.
[16] S. Kim, Y.L. Yang, A.J. Jacobson, B. Abeles, Solid State Ionics 106 (1998) 189–195.
[17] L. Wang, R. Merkle, J. Maier, T. Acartürk, U. Starke, Appl. Phys. Lett. 94 (2009) 071908.
[18] G. Kim, S. Wang, A.J. Jacobson, L. Reimus, P. Brodersen, C.A. Mims, J. Mater. Chem. 17 (2007) 2500–2505.
[19] J.P. Martínez, L.D. Marrero, C.S. Bautista, A.J.D.S. García, J.C.R. Morales, J.V. Canales, P. Nunez, Bol. Soc. Esp. Ceram. 49 (2010) 15–22.
[20] J.M. Vohs, R.J. Gorte, Adv. Mater. 21 (2009) 943–956.
[21] J.H. Lee, H. Moon, H.W. Lee, J. Kim, J.D. Kim, K.H. Yoon, Solid State Ionics 148 (2002) 15–26.
[22] M.H.D. Othman, N. Droushiotis, Z. Wu, G. Kelsall, K. Li, J. Power Sources 205 (2012) 272–280.
[23] R.Z. Liu, S.R. Wang, B. Huang, C.H. Zhao, J.L. Li, Z.R. Wang, Z.Y. Wen, T.L. Wen, J. Solid State Electrochem. 13 (2009) 1905–1911.
[24] R.Z. Liu, C.H. Zhao, J.L. Li, F.R. Zeng, S.R. Wang, T.L. Wen, Z.Y. Wen, J. Power Sources 195 (2010) 480–482.
[25] D. Ding, W. Zhu, J.F. Gao, C.R. Xia, J. Power Sources 179 (2008) 177–185.
[26] X.B. Zhu, B. Wei, Z. Lü, L. Yang, X.Q. Huang, Y.H. Zhang, M.L. Liu, Int. J. Hydrogen Energy 37 (2012) 8621–8629.
[27] J. Chen, F. Liang, D. Yan, J. Pu, B. Chi, S.P. Jiang, L. Jian, J. Power Sources 195 (2010) 5201–5205.
[28] Z.Y. Jiang, C.R. Xia, F.L. Chen, Electrochim. Acta 55 (2010) 3595–3605.
[29] Y. Huang, J.M. Vohs, R.J. Gorte, J. Electrochem. Soc. 152 (2005) A1347–A1353.
[30] L. Adijanto, R. Küngas, F. Bidrawn, R.J. Gorte, J.M. Vohs, J. Power Sources 196 (2011) 5797–5802.
[31] C.H. Zhao, R.Z. Liu, S.R. Wang, Z.R. Wang, J.Q. Qian, T.L. Wen, J. Power Sources 192 (2009) 552–555.
[32] X. Li, N.S. Xu, X. Zhao, K. Huang, J. Power Sources 199 (2012) 132–137.
[33] X.X. Meng, X. Gong, N.T. Yang, X.Y. Tan, Y.M. Yin, Z.F. Ma, J. Power Sources 237 (2013) 277–284.
[34] T. Yamaguchi, S. Shimizu, T. Suzuki, Y. Fujishiro, M. Awano, Electrochem. Commun. 10 (2008) 1381–1383.
[35] F.T. Ciacchi, K.M. Crane, S.P.S. Badwal, Solid State Ionics 73 (1994) 49–61.
[36] S.P. Jiang, J. Solid State Electrochem. 11 (2007) 93–102.